Journal of Neuroscience Research

Journal of Neuroscience Research 88:1146–1156 (2010)

Normobaric Hyperoximia Increases Hypoxia-Induced Cerebral Injury: DTI Study in Rats

K.H. Bockhorst,[1]* P.A. Narayana,[1] J. Dulin,[1] R. Liu,[2] H.C. Rea,[3] K. Hahn,[4] J. Wosik,[2] and J.R. Perez-Polo[3]

[1]University of Texas, Houston, Texas
[2]University of Houston, Houston, Texas
[3]University of Texas Medical Branch, Galveston, Texas
[4]HMGU-German Research Center for Environmental Health, Neuherberg, Germany

Perinatal hypoxia affects normal neurological development and can lead to motor, behavioral and cognitive deficits. A common acute treatment for perinatal hypoxia is oxygen resuscitation (hyperoximia), a controversial treatment. Magnetic resonance imaging (MRI), including diffusion tensor imaging (DTI), was performed in a P7 rat model of perinatal hypoxia to determine the effect of hyperoximia. These studies were performed on two groups of animals: 1) animals which were subjected to ischemia followed by hypoxia (HI), and 2) HI followed by hyperoximic treatment (HHI). Lesion volumes on high resolution MRI and DTI derived measures, fractional anisotropy (FA), mean diffusivity (MD), and axial and radial diffusivities (λ_l and λ_t, respectively) were measured in vivo one day, one week, and three weeks after injury. Most significant differences in the MRI and DTI measures were found at three weeks after injury. Specifically, three weeks after HHI injury resulted in significantly larger hyperintense lesion volumes (95.26 ± 50.42 mm^3) compared to HI (22.25 ± 17.62 mm^3). The radial diffusivity λ_t of the genu of corpus callosum was significantly larger in HHI ($681 \pm 330 \times 10^{-6}$ mm^2/sec) than in HI ($486 \pm 96 \times 10^{-6}$ mm^2/sec). Over all, most significant differences in all the DTI metrics (FA, MD, λ_t, λ_l) at all time points were found in the corpus callosum. Our results suggest that treatment of perinatal hypoxia with normobaric oxygen does not ameliorate, but exacerbates damage.

Key words: hyperoxia; ischemia; rodents; diffusivity; MRI

Perinatal hypoxia affects brain development and can have an adverse effect on motor, behavioral, and cognitive functions (Saikumar et al., 1998; Krageloh-Mann et al., 1999; Delivoria-Papadopoulos and Mishra, 2000; Levison et al., 2001; Vexler and Ferriero, 2001; Nagy et al., 2005). According to Dilenge et al. (2001) 30–50% of infants who experience perinatal hypoxia develop neurologic deficits such as epilepsy (Arpino et al., 2001; Toet et al., 2005) or cerebral palsy (Kuban and Leviton, 1994). A guideline for the treatment of acute perinatal hypoxia is resuscitation with 100% oxygen (hyperoximia) (Niermeyer et al., 2000). It has been reported that in experimental perinatal hypoxia, acute hyperoximic treatment exacerbates the initial injury (Munkeby et al., 2004; Shimabuku et al., 2005). Hu et al. (2003) reported that hyperoximia in rats triggers an additional apoptotic signaling pathway when compared to hypoxia alone. Also, elevated blood oxygen levels, as they occur during hyperoximia, decrease cerebral blood flow (Kety and Schmidt, 1946; Leahy et al., 1980; Lundstrom et al., 1995), which in turn exacerbates hypoxia-induced ischemic injury. Also, superoxide radicals can cause further tissue damage (Ditelberg et al., 1996). In summary, there are concerns whether hyperoximia is a suitable therapy for the hypoxic brain (Diringer, 2008).

The efficacy of hyperoximic treatment can be assessed in animals using the modified Rice Vannucci model (Vannucci et al., 1988; Grafe, 1994). Perinatal seven day old rat pups (P7) were subjected to ischemia followed by hypoxia (HI) only or hypoxia immediately followed by hyperoxia (HHI) (Rice et al., 1981; Barks et al., 1991; Vannucci et al., 1999; Hagberg et al., 2002). The development of rat brain at P7 is comparable to that of premature or full term infants (Vannucci et al., 1999; Hagberg et al., 2002). Therefore, HI at P7 in rats is a useful model for perinatal hypoxia in infants (Qiao et al., 2004; Olivier et al., 2005).

Contract grant sponsor: NIH Program Project; Contract grant number: 5P01HD039833 (to JRP-P); Contract grant number: NCRR/NIH S10 RR17205 (to PAN).

*Correspondence to: K.H. Bockhorst, University of Texas at Houston, Houston, Texas. E-mail: kurt.h.bockhorst@uth.tmc.edu

Received 22 May 2008; Revised 21 July 2009; Accepted 23 August 2009

Published online 2 November 2009 in Wiley InterScience (www.interscience.wiley.com). DOI: 10.1002/jnr.22273

Magnetic resonance imaging (MRI) is an excellent modality for noninvasively following changes in magnitude of lesion volumes with and without hyperoximic treatment. In addition, it is possible to assess tissue microstructural changes with diffusion tensor imaging (DTI) (Mori and Zhang, 2006). DTI has been frequently used to follow human (Neil et al., 2002; Gupta et al., 2005; Huang et al., 2006; Huppi and Dubois, 2006; Nakata et al., 2009; Berman et al., 2009; Wahl et al., 2009) and rodent brain development (Mori et al., 2001; Zhang et al., 2003, 2005; Verma et al., 2005; Sizonenko et al., 2007; Larvaron et al., 2007; Chahboune et al., 2007; Bockhorst et al., 2008; Huang et al., 2008). In a previous study, we described in detail the development of gray and white matter structures in rat brain between P0 and P56 using DTI (Bockhorst et al., 2008). In these current studies, we measured in vivo the DTI metrics, the mean diffusivity (MD), fractional anisotropy (FA), and radial (λ_t) and axial (λ_l) diffusivity of various gray and white matter structures in Wistar rat brains one day (P8), one week (P14), and three weeks (P28) after hypoxic (HI) or hypoxic and hyperoximic (HHI) treatment. We also measured lesion volumes at three weeks after injury (three weeks PI) on diffusion-weighted images and high resolution structural MRI.

MATERIALS AND METHODS

Animals and Injury Model

Pregnant Wistar rats were acquired one week prior to the expected delivery and litters culled to 10 pups to ensure that all pups had food access without competition resulting in a close gram weight for the entire litter. Pups in small litters tend to receive better care from their mother than those in larger litters. Pups raised in larger litters might therefore be more susceptible to injury than those raised in small litters. This could bias the observations made in this study. To avoid this possible bias all litters were culled to ten pups. The pups (n = 43, unsexed) were divided into three groups: naive (n = 13), HI (n = 14), and HHI (n = 16). At the age of seven days (P7) the animals of the HI and HHI group were anesthetized with isoflurane (initiation at 4%, maintenance at 2%). The left common carotid artery was ligated twice. The artery was transected between the ligatures to prevent the re-establishment of blood flow. The animals were allowed to recover for two hours and then subjected to hypoxia (90 min, 8% O_2, rest N_2) in a humidified incubation chamber (37°C). The animals of the HHI group were subsequently subjected to 100% oxygen for 120 min. A more detailed description of this procedure can be found elsewhere (Rice et al., 1981; Grafe, 1994, 2008; Hu et al., 2003, 2005, 2006).

MRI Protocol

MRI scans were performed on a 7T Bruker Biospec 30 cm (inner diameter) horizontal bore scanner (USR70/30, Bruker, Karlsruhe, Germany) equipped with a gradient insert (maximum gradient amplitude of 400 mT/m, settling time less than 80 μs). A 72-mm inner diameter volume coil was used for transmission of radio frequency (RF) power (Bruker, Karlsruhe, Germany). For improved signal-to-noise ratio (SNR), a custom-designed 22-mm outer diameter circular surface coil was used for signal reception. This coil consists of two split rings placed on two sides of a dielectric substrate (RT/Duroid 5870, Rogers Co., Chandler, AZ) to minimize the stray electric fields. The rings were rotated 180° with respect to each other. This design minimized dielectric losses due to coupling between the electric field and tissue (Kamel et al., 2007).

Animals were initially anesthetized with 4% isoflurane with an air/oxygen mixture (7:3). The isoflurane level was lowered to 1.5 ± 0.5% during the MRI scans. The animals' heads were placed in a custom built mask, connected to a mechanical ventilator (Inspira asv, Harvard Apparatus, Holliston, MA) and a Vaporizer (VMS Anesthesia Machine, MDS Matrix, Orchard Park, NY). The pups' body temperature was maintained at 36 ± 1°C with a feedback controlled warm air system (SA Instruments, Stony Brook, NY). The respiration rate and surface body temperature were continuously monitored (SA Instruments, Stony Brook, NY). Blood oxygen saturation and heart rate were measured with a pulse oximeter (NONIN, Plymouth, MN). The survival rate in these longitudinal studies was approximately 95%. MRI scans were performed one day, one week, and three weeks post-injury (PI).

All animal procedures were performed in accordance with the guidelines published in NIH 'Guide for the Care and Use of Laboratory Animals' and the principles presented in the *Guidelines for the Use of Animals in Neuroscience Research* (Society of Neuroscience). The procedures were approved by our institutional Animal Welfare Committee.

Anatomical Images

A 'tripilot' scan, which acquires simultaneously three slices in coronal, sagittal, and axial orientations, was used for positioning and prescribing the subsequent scans. 'Fastmap' (ParaVision, Bruker, Karlsruhe, Germany), an automatic procedure, was applied for shimming the magnetic field. Multislice, contiguous coronal images were acquired with dual echo RARE (Rapid Acquisition and Relaxation Enhancement) sequence with the following parameters: first echo time (TE1)/second echo time (TE2)/repetition time (TR) = 22 msec/66 msec/5 sec; RARE factor = 4; slice thickness = 0.5 mm; square field-of-view (FOV) = 35 mm; acquisition matrix = 256 × 192, which was zero filled to 256 × 256, number of averages = 2. The number of contiguous slices was between 20 and 40, depending on the size of the brain. The spatial resolution was 0.137 mm × 0.137 mm × 0.5 mm. The acquisition time was 8 min.

Diffusion Tensor Imaging

Diffusion-weighted images (DWI) were acquired with a four-shot spin-echo EPI sequence. The geometry and location of the scan was imported from the RARE scan. A rotationally-invariant icosahedral encoding scheme with 21 alternating polarity encoding directions (total number of encoding directions = 42) (Madi et al., 2005) was used. The acquisition parameters were: TE/TR = 38 ms/4000 msec; diffusion gradient pulse duration, δ = 2.3 msec; gradient separation,

Δ = 22 msec, sweep width = 200 kHz; acquisition matrix = 128 × 128, spatial resolution of 0.27 mm × 0.27 mm × 0.5 mm, number of repetitions = 9 with b = 0 (reference or b0 images), number of repetitions = 4 with diffusion-weighting per encoding direction. The average acquisition time for the DTI data was 35 min.

MRI Data Processing

All data processing was performed on a PC (Dell, Pentium 4, 3 GHz, 2 GB RAM) operating under Windows XP. Diffusion-weighted images generally suffer from ghosting that needs to be minimized. Ghosts in MRI are signals which are spatially misplaced during the image reconstruction. One type of ghosting in segmented ('multi shot') EPI occurs because of the interaction between eddy currents and time delay in focusing of the even and odd echoes. The second type of ghosting occurs because of subject motion (breathing, movement), or physiological motion (perfusion, blood flow). Digital tuning is a method to correct both types of ghosts (Ye and Xiang, 2007). For inter-segment tuning, it is assumed that the phase in the first segment is correct while the phase in other segments needs correction. Phase correction was performed in the time domain, involving two tuning parameters for each segment. For even-odd echo tuning, kx lines in the k space were first sorted into even and odd echo groups, then Fourier transformed along the x-direction. Zero and first order phase corrections were applied along the x-direction in the k space. After both, inter-echo and inter-segment phase corrections, a magnitude image was reconstructed. Across this image, total variation (TV) was computed as the L1 norm of its gradient. Minimization of total variation provided the optimal tuning parameter set which was then used to reconstruct the final image. The digital tuning program was provided by Ye and Xiang (Ye and Xiang, 2007) and it was embedded into batch jobs written in IDL language (ITT Visual Information Solutions, Boulder CO). A library routine was used for multidimensional minimization with the downhill simplex method. The corrected FIDs (Free Induction Decay, MRI raw data) were reconstructed using the ParaVision (Bruker, Karlsruhe, Germany) macro 'FRECO'. Remaining ghosts were automatically identified in the magnitude images using SNR measurements at the center of mass ('signal') and at the edges of the image in xy direction ('noise'). Ghosted images were replaced by unghosted images. The images were magnitude-averaged and automatically cropped to a 71 × 71 matrix to shorten the data processing time. The data were smoothed and denoised, assuming a Rician distribution for noise. The code for denoising was provided by Hahn et al., (Hahn et al., 2009) and embedded into batch jobs written in IDL language (ITT Visual Information Solutions, Boulder, CO). Extrameningeal tissues were manually cropped on b0 images using ImageJ (NIH, Bethesda, MA). The resulting images were transformed into a mask, which was applied to the complete diffusion-weighted image data set. The diffusion-weighted images were warped (second order nonlinear 30 parameter 3D model) to the corresponding b0 images using AIR (Woods et al., 1998a, 1998b). All processing steps (except the manual stripping of extrameningeal tissue) were fully automatic and processed as batch jobs, which reduced user bias and processing errors.

DTI Measures

The maps of the DTI metrics MD, λ_l, λ_t, and FA were generated from the preprocessed DWI data sets using DtiStudio (Johns Hopkins University, Baltimore, MD). The information derived from the spatially encoded diffusivities was used to calculate the three eigenvalues. The largest eigenvalue represents the longitudinal diffusivity, λ_l. The eigenvalues along the x and y direction were averaged to calculate the radial diffusivity, λ_t. The FA (fractional anisotropy) reflects the overall diffusion anisotropy. The MD (mean diffusivity) reflects the diffusion coefficient averaged over all directions. The DTI metrics of various structures were measured using the 'ROI Manager' (ImageJ). This allowed the measurements of identical ROIs in different parametric maps. The results were imported into Excel spreadsheets.

The measurements were focused on four gray matter structures (hippocampus (hi), caudate putamen (cpu), cortical plate (cp), cortical mantle (cm) and seven white matter structures: body (bcc), genu (gcc), and splenium (scc) of corpus callosum, external (ec) and internal capsule (ic), fimbria (fi), and cingulum (cg).

DTI measures were performed on three slices, which included either scc (∼bregma −5 mm), or fi, ic, and bcc (∼bregma −1 mm), or gcc (∼bregma +2 mm). All structures were identified by comparing both anatomical images and FA maps with the Paxinos and Watson atlas (Paxinos and Watson, 2005). Measurements were performed exclusively in the contralateral hemisphere because of the severe damage in the ipsilateral hemisphere especially after HHI. Measurements of the cortical mantle (close to the external capsule) and the cortical plate (close to the dura) were performed at a superior (∼somatosensory cortex S1) and an inferior position (∼somatosensory cortex S2) in the slice containing the bcc. The DTI metrics were performed on 15 ROIs per animal.

Lesion Volume

Two types of lesions were included in the analysis: 1) hyperintense lesions on MD maps and 2) hypointense on T2-, Proton-density, and DWI images. In animals with injured brain tissue, edema and cysts are present and show elevated MD values. The volumes with elevated MD values were detected automatically by setting the threshold to 1.0×10^{-3} mm^2/sec, consistent with reported literature values (Koinig et al., 2000). The number of pixels exceeding this threshold was counted using a global histogram function (ImageJ). This procedure worked consistently on all the animals and eliminated any operator bias. The same procedure for segmenting lesions appearing hypointense on MR images did not work consistently. Therefore, volumes of these lesions were measured manually by two operators independently by defining regions of interest (ROI) and stripping them of surrounding pixels. The number of pixels inside the ROIs was counted using a global histogram function (ImageJ).

Histology

The rat pups were deeply anesthetized with 150 mg/kg intraperitoneal nembutal (Ovation Pharmaceuticals, Deerfield, Il) and perfused transcardially with 0.9% saline flush followed by 4% buffered paraformaldehyde in PO_4 buffer. The brains were removed and incubated in paraformaldehyde overnight at 4°C. The midbrain was blocked, dehydrated with EtOH and then embedded in paraffin. Coronal blocks were sectioned at 8 μm.

Myelin and Phospholipids

Following deparaffinizing and hydration, brain sections were stained using 0.1% Luxol fast blue stain (Sigma-Aldrich, St. Louis, MO cat # S3382). Slides were incubated in Luxol blue for 30 min at 80°C then cooled at room temperature for another 30 min. Excess stain was rinsed with 95% EtOH for 5 min followed by tap water wash. Slides were differentiated 30 sec in 0.05% lithium carbonate solution and rinsed in 70% EtOH. The slides were washed with distilled water and then counterstained for 40 sec with 0.1% Cresyl violet neuronal stain (Sigma-Aldrich). Slides were washed, dehydrated with EtOH, xylene and coverslipped.

Iron

Tissue sections were deparaffinized and rehydrated with decreasing concentrations of ethanol, then washed in distilled water. To detect iron-positive cells, slides were incubated in Perl's Prussian Blue Stain (2% aqueous potassium ferrocyanide-hydrochloric acid, 15 min), followed by neutral red stain for visualization of cell bodies (1 min). Following staining, slides were washed in distilled water, dehydrated, cleared with Hemo-De solvent (Fisher Scientific, Pittsburgh, PA), and coverslipped with mounting media.

Fluorescent Immunolabeling

Tissue sections were washed and rehydrated in TBS, blocked in 5% normal goat serum, and incubated with anti-GFAP (anti-glial fibrillary acidic protein, 1:1000, Dako, Carpinteria, CA) overnight at 4°C. Next day, tissue was washed, incubated in AlexaFluor-conjugated goat anti-rabbit antibody (1:500, Molecular Probes, Eugene, OR), and washed again with TBS. Sections were coverslipped with Fluoromount mounting media (Electron Microscopy Sciences, Hatfield, PA).

Statistical Analysis

The significance of the differences between hypointense lesions was calculated with an unpaired t-test ($p < 0.05$). The significance of the differences between hyperintense lesions was calculated with a one-way ANOVA test ($p < 0.05$). The significance of the difference of DTI metrics was calculated with a two-way ANOVA test ($p < 0.05$). Bonferroni post-tests were applied to determine the groups which showed significant differences. All calculations were performed with Prism software (GraphPad, La Jolla, CA). The values are reported as means ± standard deviation (Mean ± S.D.)

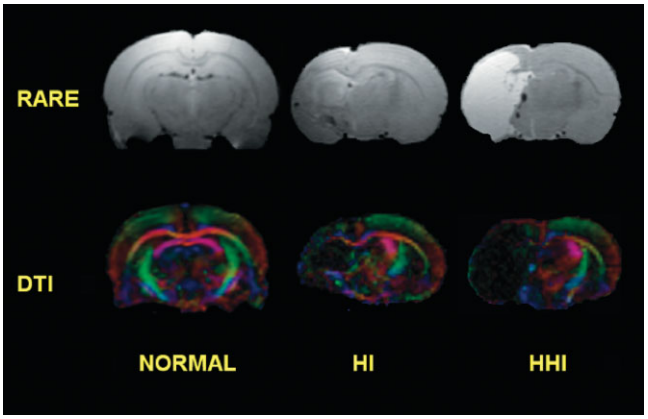

Fig. 1. Displayed are naive (left), HI (middle), and HHI animals (right) three weeks PI (P28). The top row presents anatomical RARE images, the bottom row color coded FA maps. Red corresponds to structures with high anisotropy in the left-right, blue in the rostral-caudal, and green in the dorsal-ventral orientation. The FA maps show severe damages of most structures in the ipsilateral hemisphere in HI and even more severe in HHI animals. Also, the structures of the contralateral hemisphere appear diffuse in HI and HHI animals in contrast to the naive brain (bottom left). The HHI case (top right) exhibits hypointense lesions at the border between edema and naive tissue.

Results

Figure 1 displays a naive (left), HI (middle), and HHI animal (right) at three weeks PI (P28). We observed most significant differences in the DTI measures in white matter structures (see below). Therefore, we chose the section shown in Figure 1 that corresponds to location one millimeter posterior to the bregma and shows a large number of white matter structures. The top row presents anatomical RARE images and the bottom row shows color coded FA maps calculated from the DTI data. In the color coded FA maps, red corresponds to the principal axis along the right-left, blue along the rostral-caudal, and green along the dorsal-ventral directions. The brains of three-week old pups have almost the size of those of adult rats and therefore show the typical intensity gradient that is inherent to surface coils. Visually it is apparent that the brain volumes of HI and HHI animals are smaller than those of controls. The corresponding FA maps show severe damage to several brain structures in the ipsilateral hemisphere in HI and even more severe in HHI animals. After HHI (bottom right) almost no anisotropic structures were seen in the ipsilateral hemisphere. Also, the structures in the contralateral hemisphere appear diffuse in HI and HHI animals, in contrast to naïve brains (bottom left). The HHI animals (top right) exhibit hypointense lesions in the neocortex and thalamus. The edema in the HHI animals appeared much brighter than in the HI case (middle of top row). Its brightness was comparable to that of the CSF, indicating the cystic nature of the lesions.

Lesion Volumes

Two out of five HI animals and all four HHI animals (three weeks PI) displayed large volumes with elevated MD

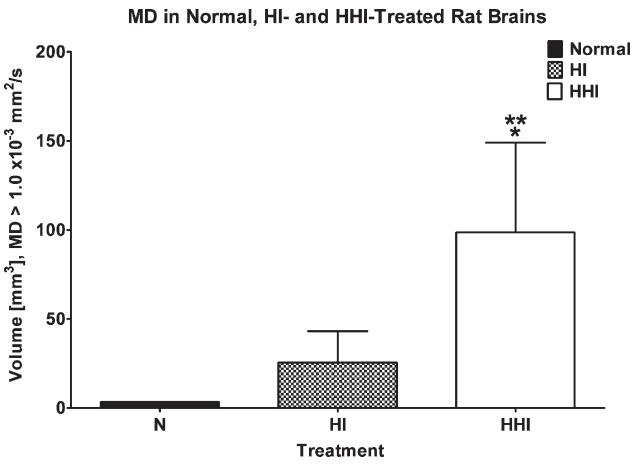

Fig. 2. HI (middle, 25.53 ± 17.62 mm^3) and HHI (right, 98.56 ± 50.42 mm^3) produced significantly different sizes of volumes with elevated MD values (one-way ANOVA with Bonferroni post test, $p < 0.05$). These volumes need to be corrected for ventricles with the corresponding volume measured in naive animals (left, 3.30 ± 0.22 mm^3) to be considered as pure lesions. A threshold of 1.0×10^{-3} mm^2/sec was chosen to discriminate between naive tissue (MD $\sim 0.8 \times 10^{-3}$ mm^2/sec) and edematous lesions.

($>1.0 \times 10^{-3}$ mm^2/sec; Koinig et al., 2000) in the ipsilateral hemisphere at three weeks PI. The difference among the average volumes was significant between naives and HHI, but not between naives and HI animals (ANOVA, Bonferroni post test; Fig. 2). Volumes with elevated MD in naive animals are the ventricles (3.30 ± 0.22 mm^3). The average volumes of hyperintense appearing lesions were 25.53 ± 17.62 mm^3 in HI and 98.56 ± 50.42 mm^3 in HHI animals. Animals with large volumes of elevated MD also showed hypointense areas on T2-, DWI-, and proton density-weighted images, mostly in the ipsilateral superior and lateral cortex and the lateral thalamus. These areas were quantified by manually drawing regions of interest (ROIs) and calculating the volume using ImageJ (NIH, Bethesda, MA). There is a high degree of concordance between the hypointense volumes determined by both the operators (intraclass correlation = 0.96). The average volumes of the hypointense lesions were 16.8 ± 23.1 mm^3 (HI) and 41.3 ± 17.9 mm^3 (HHI). The volume of the hypointense lesion was higher in HHI compared to HI, but this difference did not reach statistical significance (unpaired t-test, $p = 0.07$). The lesions occur mainly in gray matter structures, which are underrepresented at the slice location shown in Figure 1 and therefore appear smaller than expected from the results presented above.

DTI Metrics

The FA of gcc was significantly different between HI and naive animals. The FA of scc, ec, and gcc was significantly different between naive and HHI animals (Fig. 3, Table I). The differences in FA between HI and HHI were not significant in any structure.

Figure 4 displays the radial diffusivities λ_t for naive, HI, and HHI animals three weeks after injury. The differences in

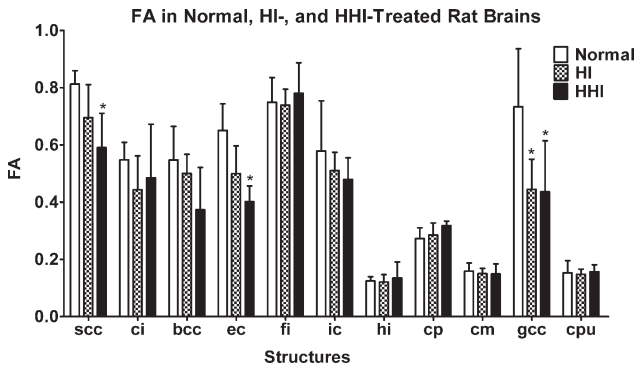

Fig. 3. Displayed is the fractional anisotropy FA for naive, HI, and HHI animals in several brain structures. Gcc was significantly different between naive and HI animals three weeks post-HI. Significant differences were also found between naive and HHI animals in scc, ec, and gcc ($p < 0.05$, two-way ANOVA, Bonferroni post test).

TABLE I. Significantly different DTI metrics in cerebral structures three weeks post injury

	DTI Metrics			
Structures	λ_t	FA	MD	λ_l
gcc	b	a,b	c	a
bcc	b,c	–	b,c	b
scc	b	b	–	–
ec	b	b	–	–
cpu	–	–	c	–

Table I summarizes the significant differences of all DTI metrics found in cerebral structures three weeks post hypoxic insult (HI) or hypoxic insult followed by hyperoximia (HHI). Most significant differences were found in the structures of the corpus callosum (two-way ANOVA with Bonferroni post test, $p < 0.05$; a, HI vs naive; b, HHI vs naive; c, HI vs HHI). Additionally to the corpus callosum, ec and cpu had significant differences.

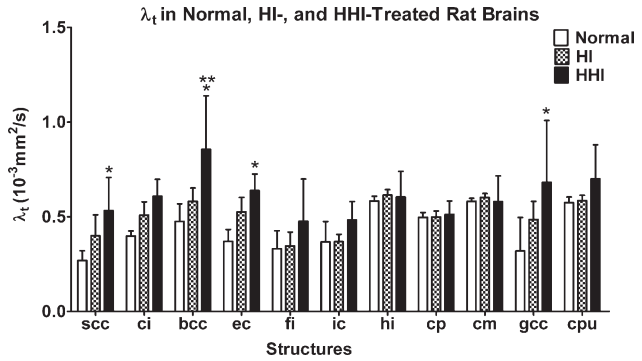

Fig. 4. Radial diffusivities λ_t in naive, HI, and HHI animals three weeks after injury: Significant differences were found in scc, bcc, ec, and gcc between naive and HHI animals. Additionally, bcc was significantly different between HI and HHI animals ($p < 0.05$, two-way ANOVA, Bonferroni post test). The differences between naive and HI animals were never significant in any structures observed.

λ_t between naive and HI animals were not significant in any gray or white matter structures. In contrast, the differences between naive and HHI animals were significant for scc, bcc, ec, and gcc. The difference of λ_t between HI and HHI animals was significant for bcc (Fig. 4, Table I).

The MD values of bcc were significantly different between naive and HHI, or HI and HHI animals (Table I). Also, the MD of the cpu and gcc were significantly different between HI and HHI rats.

The axial diffusivity λ_l was significantly different in bcc (HHI vs naive) and gcc (HI vs. naive, Table I).

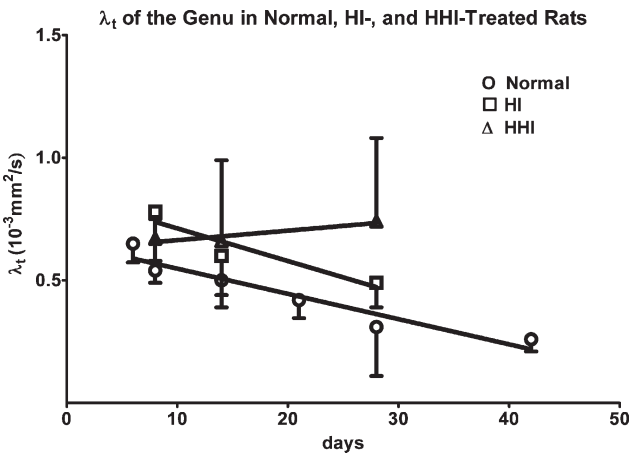

Fig. 5. Displayed is the development of λ_t in the genu of naive, HI, and HHI animals. The λ_t of naive animals (O) shows a linear decreasing trend over the selected time frame. HI animals (□) show also a trend to decreasing values over the time but at slightly larger values indicating demyelination. In contrast to naive and HI, HHI animals (Δ) showed an increasing trend indicating a poor prognosis.

Temporal Evolution

We assessed the serial changes in the DTI measures in different brain structures on day one (P8), one week (P14), and three weeks (P28) PI. Few significant differences in the DTI metrics were observed during the first week after injury. The FA and λ_t of gcc were significantly different on day one (naive vs HI). The FA of scc was significantly different at one week (naive versus HHI). All significant differences during the first week occurred in the corpus callosum. Most significant differences were found three weeks PI: gcc, ec, bcc, scc, and cpu (Table I).

Evolution of Radial Diffusivity in gcc

Figure 5 displays the temporal trajectory of λ_t in gcc of naive, HI, and HHI animals. The λ_t of naive animals showed a linear decreasing trend over the selected time frame. HI animals also showed a trend of decreasing λ_t that almost parallels the trend observed in naives although larger λ_t values were observed in HI animals compared to naives. This positive offset of λ_t in HI animals indicates less hindered diffusion normal to the fiber orientation, that could result from a smaller degree of myelination (Song et al., 2002). In contrast to naive or HI animals, the λ_t of gcc in HHI animals showed an increasing trend over time. The differences between naive and HHI animals displayed at P28 were significant (Figs. 3, 4).

Histology and DTI

Figure 6 shows myelin staining of the ec of a naive (A), HI (B) and HHI animal (C, three weeks PI). The HI animal did not show significant differences compared to a naive animal. The corresponding λ_t value of the HI group was not significantly different compared to the naive group (two way ANOVA, Bonferroni post test, Fig. 4). The contralateral ec of the HHI animals clearly showed dead cells and tissue loss (C). The corresponding λ_t value of the HHI group was significantly different from that of the naive group (Fig. 4).

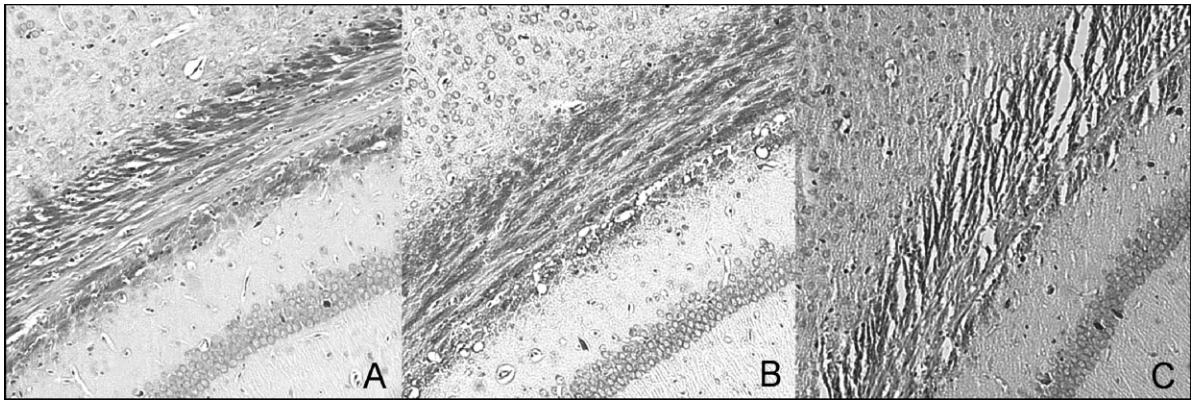

Fig. 6. Histological sections (myelin Luxol Fast Blue stain) of the ec of a representative naive (**A**), HI (**B**), and HHI animal (**C**) three weeks after injury (P28). The sections of the naive and HI animals did not show differences. The cells of the HI animal appeared naive (B). In agreement, the corresponding λ_t values of the naive and HI groups were not significantly different. The ec of the HHI pup appeared clearly damaged exhibiting dead cells and tissue loss (C). The corresponding λ_t value of the HHI group was significantly different from the naive value ($p < 0.05$, two-way ANOVA, Bonferroni post test).

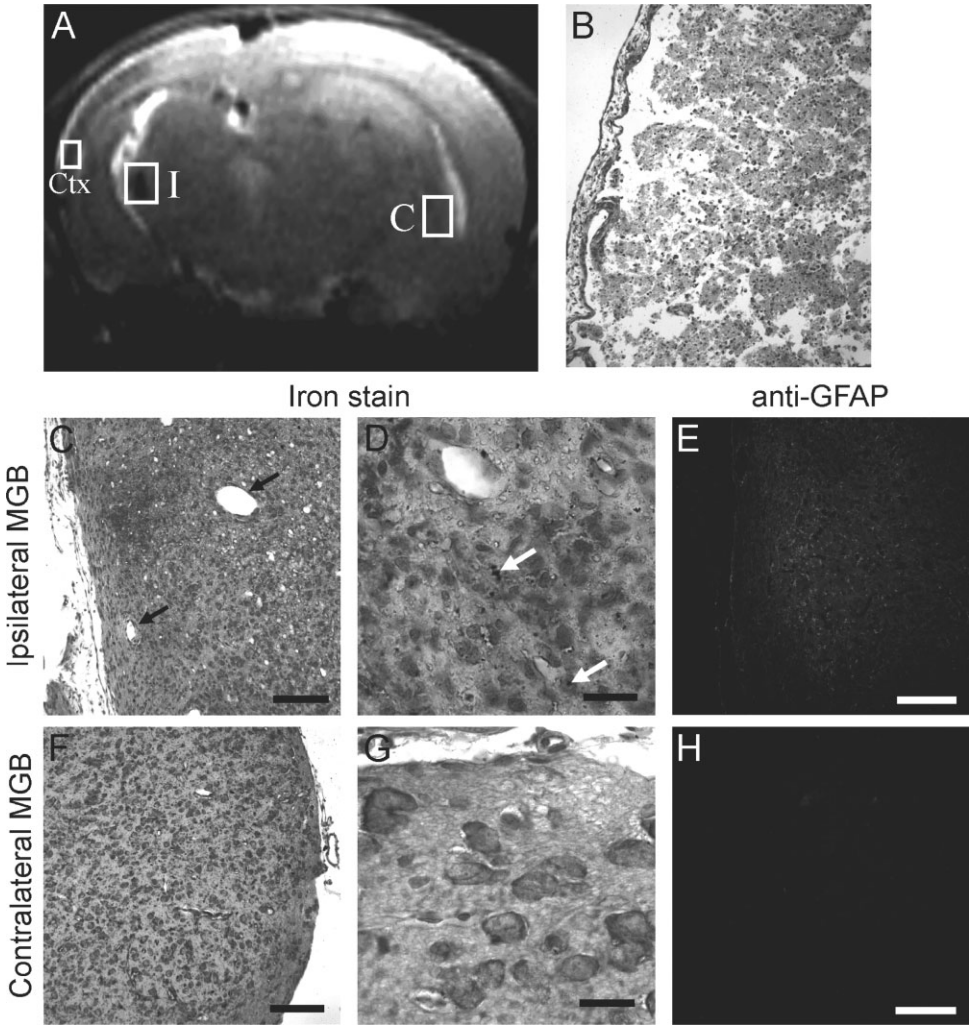

Fig. 7. Hypointense MR regions correspond to localized astrogliosis in a 3 weeks post-HHI subject. MR image of axial HHI brain, approx. bregma −5.5 mm (**A**). Box marked "I" corresponds to ipsilateral medial geniculate body (MGB) of thalamus (C-E); box marked "C" corresponds to contralateral MGB (F-G); box marked "Ctx" corresponds to cortex (**B**). B: 10× magnification of iron-stained cortical tissue, showing extensive tissue loss. **C-H**: Immunohistochemical staining of axial HHI brain sections. C, F: Cell bodies (gray) stained for iron (black), 10× magnification. D, G: 60× magnification. C: Holes in tissue indicate vascularization (black arrows). D: Iron particles are marked by white arrows. E, H: GFAP+ astrocytes (gray) clustering in the ipsilateral MGB but not seen in the contralateral. Scale bars: 150 μm (C, E, F, H); 20 μm (D, G).

To determine the pathological nature of regions displaying localized MR hypointensities, we performed histological staining on coronal brain sections (3 weeks post-HHI). We first examined the region of cortical tissue appearing hypointense on the MRI (Fig. 7A, Ctx). Staining for neuronal cell bodies revealed extensive loss of tissue from cortex (Fig. 7B) closely corresponding with hypointensities on proton density, T2-weighted, DWI images. Tissue loss was not apparent in the ipsi- or contralateral medial geniculate body (MGB) of the thalamus (Fig. 7C,F). We hypothesized that high tissue iron content associated with hemorrhage could have resulted in hypointense signals in the ipsilateral MGB. To test this, we stained tissue sections for presence of iron. The ipsilateral MGB showed increased levels of iron reactivity. Specifically, we observed that cell bodies contained more intracellular iron particles (Fig. 7D, white arrows) than those of the contralateral MGB. Morphologically, we observed that cells in the ipsilateral tissue were more densely localized in the MGB than surrounding regions. This uneven distribution of cells compared to the contralateral MGB is consistent with an injury-induced disruption in local cytoarchitecture. Additionally, the ipsilateral thalamus displays greater vascularization (Fig. 7C, black arrows). It has been well documented that hypervascularity coincides with astroglial scar formation following CNS injury (Blight, 1991; Stichel and Muller, 1998). We hypothesized that such gliosis could therefore be implicated in the hypointense MR signal of the ipsilateral thalamus. We performed fluorescent immunolabeling with an antibody to glial

fibrillary acidic protein (GFAP), an intermediate filament protein expressed in astrocytes. We observed a clear clustering of GFAP+ cells in the ipsilateral MGB and cortex (not shown), but not in the contralateral (Fig. 7E,H). These observations taken together provide a strong evidence of astroglial scar formation in the ipsilateral thalamus and cortex.

DISCUSSION

Injury after HI

There was a significantly decreased FA only in the genu (0.44 ± 0.11) three weeks post-HI (naive: 0.73 ± 0.20, Fig. 5). Also, the λ_l of the genu was significantly smaller at three weeks post-HI (not shown). Decrease in axial diffusivity λ_l is considered as an indicator of axonal damage (Song et al., 2003). In humans perinatal hypoxia has significant effects on corpus callosum size, especially the genu (Maneru et al., 2003). Nagy et al reported a decreased anisotropy of the corpus callosum and other white matter structures (Nagy et al., 2005). A correlation between anisotropy and myelination was confirmed by Sakuma and Rutherford (Rutherford et al., 1991; Sakuma et al., 1991).

Wang et al. (2008) measured DTI metrics in the ec one day and one week post-HI in rats. They reported FA of 0.38 ± 0.06 (one week post-HI, contralateral, 'non-cystic group') compared to 0.46 ± 0.10 (one week post-HI). The corresponding λ_t was $630 \pm 60 \times 10^{-6}$mm^2/sec (Wang et al.) compared to $620 \pm 211 \times 10^{-6}$mm^2/sec (one week post-HI). These results are in good agreement with each other. Wang et al. (2008) did not report DTI metrics for naive animals or any structures other than the ec and did not report absolute lesion values.

Sizonenko et al. (2007) reported cortical DTI data on naive pups at P6, with FA values of 0.36 ± 0.07 for cortical plate and 0.21 ± 0.02 for cortical mantle. We found at P8 an FA of 0.25 ± 0.04 in the cortical plate and 0.11 ± 0.02 in the cortical mantle. Sizonenko et al. (2007) also found an FA in P6 rat cortex, three days post-HI, of 0.27 ± 0.01 to our FA of 0.19 ± 0.07 (one day post-HI), both averaged over cortical mantle and plate, contralateral hemisphere. The strong decline in cortical FA during the first week after birth may explain these differences (Bockhorst et al., 2008; Huang et al., 2008).

Injury after HHI

These are the first in vivo DTI reports on the effect of hyperoximia on hypoxia ischemia. The most significant differences in DTI metrics were at 3 weeks post-HHI (Figs. 3 and 4, Table I), particularly in the genu (FA = 0.73 ± 0.20 in naive vs, 0.44 ± 0.18 in HHI, $p < 0.05$). Also, the ec showed significantly lower FA (0.65 ± 0.09 in naive vs 0.40 ± 0.06 in HHI, $p < 0.05$) and increased λ_t values ($370 \pm 60 \times 10^{-6}$mm^2/sec in naive vs $640 \pm 90 \times 10^{-6}$ mm^2/sec in HHI, $p < 0.05$; Table I). HI alone affected the FA and λ_l only in the gcc. HHI clearly increased the number of structures in which significant differences in λ_l were observed compared to naives. The volume of the hyperintense lesions after HHI was significantly larger compared to HI alone (3 weeks PI, Fig. 2) similarly to results reported elsewhere for one day post-injury (Gill et al., 2008) that showed larger cortical damage than previous reports (Shimabuku et al., 2005) where there was brain damage in 42% of rats treated with HHI and 13% of those treated with HI. We report that HI caused lesions in 60% of rats and HHI caused lesions in 100% of all rats. The differences between the two studies may reflect differences in the carotid artery ligation protocols. We used double ligation and additional dissection to prevent re-establishment of blood flow and kept rats at a different temperature compared to Shimabuku et al. (2005), since lower temperatures have been shown to be neuroprotective in ischemic events (Lyden et al., 2006).

A rationale for the worsening outcome after the hyperoximic treatment was suggested by Hu et al. (2003), who followed three apoptotic markers (cytoplasmic histone/DNA, caspase 3 activities, and Klenow fragments) after HI and HHI and found that hyperoximia induced an additional apoptotic pathway to the one induced by HI. Also, hyperoximia decreased CBF by 10–30% (Kety and Schmidt 1946; Rostrup et al., 1995; Watson et al., 2000; Nishimura et al., 2007; Zaharchuk et al., 2008), perhaps due to vasoconstriction (Nakajima et al., 1983; Watson et al., 2000). Such reductions in CBF are not likely to be harmful except to poorly perfused ischemic tissue (Watson et al., 2000; Fumagalli et al., 2004).

Normobaric hyperoximia is reported to be neuroprotective in experimental cerebral ischemia in healthy adult animals, which may be less susceptible to HI or HHI than pups (Branston et al., 1976; Kaminogo 1989; Shin et al., 2007). The perinatal development of the brain is especially vulnerable to hypoxic ischemic injury (Rice and Barone, 2000), which might explain the noxious effect of hyperoximia to neonates in contrast to adults.

Calvert and Zhang (2007) reported that oxygen treatment improved energy restoration (ATP-, phosphocreatine-, and glucose-levels) after HI in neonatal rats within 72 hr after HI. However, there are HI-induced transient changes in brain that usually disappear within two weeks (Mader et al., 2002; Kuker et al., 2004; Barkovich et al., 2006; Meng et al., 2006). Therefore the reported improvements in energy restoration may only be a transient effect.

A more recent study on the effects of HI and HHI on gray matter structures in the P7 rat model concluded that while 100% oxygen vs. room air (21% oxygen) does not significantly improve outcome, 40% oxygen versus 21% or 100 % oxygen was beneficial (Grafe et al., 2008). Grafe's study focused on neocortex, caudate putamen, hippocampus, and thalamus at six weeks post-injury but did not include white matter. We did not detect significant differences in gray matter although these might have been significant beyond our observation period.

DTI

The DTI acquisition and processing techniques employed in our study are both robust and sophisticated. The applied encoding scheme with 42 directions is rotationally invariant, which reduces estimation bias of the results (Madi et al., 2005). Ghosted data was corrected in the k-space using digital tuning (Ye and Xiang, 2007), in which the phase of the first EPI segment is used to correct the remaining segments. Further deghosting was performed on magnitude images calculating SNR ratios. Also, the magnitude images were smoothed and denoised assuming a Rician distribution for the noise (Hahn et al., 2009). We acquired four averages for each encoding direction and nine averages for b_0 references. Weighted images were warped to the unweighted images using AIR (Woods et al., 1998a, 1998b) to reduce artifacts induced by eddy currents. Finally, as described by Madi et al. (2005), the rigorous quality control program that is implemented on our scanner assures high temporal stability that is critical for the DTI studies. Since DTI is a modality with relatively poor signal-to-noise ratio, voxel sizes were limited to $0.27 \times 0.27 \times 0.5$ mm. Partial volume effects were unavoidable, especially in thin structures such as the external capsule. Partial volume effects would result in decreased fractional anisotropy of white matter structures. However, the FA values we observed were at the higher end of that reported in the literature, suggesting that our results are not significantly affected by partial volume effects.

Histology

Lesions appearing hyperintense on T2-weighted MRIs are generally attributed to edema. We used mean diffusivity to quantify the volume of hyperintense lesions. Hypointense lesions, despite their relatively large sizes could not be quantified in a similar manner because of the low contrast in DTI measures (Schroeter et al., 2001). We therefore correlated hypointense regions of MRI with histological imaging, to better describe HHI effects on the developing CNS, an approach used in models of ischemia and hypoxia (Schroeter et al., 2001). However, we did not find studies that compared MRI with pathological changes in a postnatal HHI model extending beyond two weeks post-injury. Our observations provide evidence for localized tissue loss and astroglial scarring after HHI in postnatal rat pups. Increased vascularization, disruption of the cytoarchitecture, and localized GFAP expression indicate gliosis in the MGB of the ipsilateral HHI thalamus. However, the contribution of gliosis to regions of hypointense MRI signal is unclear. We propose that at 3 weeks post-HHI, areas of increased iron due to hemorrhage may account for the marked hypointensities observed in specific CNS regions. Iron staining results support this hypothesis; however, tissue iron immunoreactivity was lower than that of hemorrhagic tissue. This discrepancy is likely be attributed to the vascular saline flush during tissue processing. Alternatively, astrocytes have been shown to upregulate production of ferritin, an iron-sequestering protein, in response to increased extracellular iron levels coincident with oxidative injury (Regan et al., 2002). It is then possible that the decreased MRI signal intensity is due in part to increased intracellular iron-bound ferritin within the astroglial population.

CONCLUSIONS

We have shown in these in vivo DTI studies that there is significant injury to the corpus callosum genu, three weeks post-HI. Hyperoximia, followed by HI, significantly increased the severity of this white matter damage by extending it to adjacent structures as bcc, scc, and ec. Also, hypointense appearing lesions on T2-, proton-density-, and diffusion-weighted MRIs were significantly larger after HHI than after HI alone. Volumes with elevated MD were also significantly larger after HHI than after HI alone. The radial diffusivity, fractional anisotropy, and the lesion volumes indicate a significant worsening of outcome if HI is treated with hyperoximia (100% O_2). The extrapolation of the temporal development over the period studied here predicts a further increase of the injury at later time points. The increase of the radial diffusivity indicates demyelination, which is considered as a severe pathologic event concerning neurological functions. Thus, we conclude that hyperoximic treatment of HI does significantly worsen the prognosis in perinatal animals.

ACKNOWLEDGMENTS

We thank Drs. F.Q. Ye and Q.-S. Xiang for providing the digital tuning software, Cheukkai Hui for his help with data analysis, and Dr. Raymond Grill for discussing the histology.

REFERENCES

Arpino C, Domizio S, Carrieri MP, Brescianini DS, Sabatino MG, Curatolo P. 2001. Prenatal and perinatal determinants of neonatal seizures occurring in the first week of life. J Child Neurol 16:651–656.

Barkovich AJ, Miller SP, Bartha A, Newton N, Hamrick SE, Mukherjee P, Glenn OA, Xu D, Partridge JC, Ferriero DM, Vigneron DB. 2006. MR imaging, MR spectroscopy, and diffusion tensor imaging of sequential studies in neonates with encephalopathy. AJNR Am J Neuroradiol 27:533–547.

Barks JD, Post M, Tuor UI. 1991. Dexamethasone prevents hypoxic-ischemic brain damage in the neonatal rat. Pediatr Res 29:558–563.

Berman JI, Glass HC, Miller SP, Mukherjee P, Ferriero DM, Barkovich AJ, Vigneron DB, Henry RG. 2009. Quantitative fiber tracking analysis of the optic radiation correlated with visual performance in premature newborns. AJNR Am J Neuroradiol 30:120–124.

Blight AR. 1991. Morphometric analysis of blood vessels in chronic experimental spinal cord injury: hypervascularity and recovery of function. J Neurol Sci 106:158–174.

Bockhorst KH, Narayana PA, Liu R, Ahobila-Vijjula P, Ramu J, Kamel M, Wosik J, Bockhorst T, Hahn K, Hasan KM, Perez-Polo JR. 2008. Early postnatal development of rat brain: in vivo diffusion tensor imaging. J Neurosci Res 86:1520–1528.

Branston NM, Symon L, Crockard HA. 1976. Recovery of the cortical evoked response following temporary middle cerebral artery occlusion in baboons: relation to local blood flow and P_{O_2}. Stroke 7:151–157.

Calvert JW, Zhang JH. 2007. Oxygen treatment restores energy status following experimental neonatal hypoxia-ischemia. Pediatr Crit Care Med 8:165–173.

Chahboune H, Ment LR, Stewart WB, Ma X, Rothman DL, Hyder F. 2007. Neurodevelopment of C57B/L6 mouse brain assessed by in vivo diffusion tensor imaging. NMR Biomed 20:375–382.

Delivoria-Papadopoulos M, Mishra OP. 2000. Mechanisms of perinatal cerebral injury in fetus and newborn. Ann N Y Acad Sci 900:159–168.

Dilenge ME, Majnemer A, Shevell MI. 2001. Long-term developmental outcome of asphyxiated term neonates. J Child Neurol 16:781–792.

Diringer MN. 2008. Hyperoxia: good or bad for the injured brain? Curr Opin Crit Care 14:167–171.

Ditelberg JS, Sheldon RA, Epstein CJ, Ferriero DM. 1996. Brain injury after perinatal hypoxia-ischemia is exacerbated in copper/zinc superoxide dismutase transgenic mice. Pediatr Res 39:204–208.

Fumagalli M, Mosca F, Knudsen GM, Greisen G. 2004. Transient hyperoxia and residual cerebrovascular effects in the newborn rat. Pediatr Res 55:380–384.

Gill MB, Bockhorst K, Narayana P, Perez-Polo JR. 2008. Bax shuttling after neonatal hypoxia-ischemia: hyperoxia effects. J Neurosci Res 86: 3584–3604.

Grafe MR. 1994. Developmental changes in the sensitivity of the neonatal rat brain to hypoxic/ischemic injury. Brain Res 653:161–166.

Grafe MR, Woodworth KN, Noppens K, Perez-Polo JR. 2008. Long-term histological outcome after post-hypoxic treatment with 100% or 40% oxygen in a model of perinatal hypoxic-ischemic brain injury. Int J Dev Neurosci 26:119–124.

Gupta RK, Hasan KM, Trivedi R, Pradhan M, Das V, Parikh NA, Narayana PA. 2005. Diffusion tensor imaging of the developing human cerebrum. J Neurosci Res 81:172–178.

Hagberg H, Ichord R, Palmer C, Yager JY, Vannucci SJ. 2002. Animal models of developmental brain injury: relevance to human disease. A summary of the panel discussion from the Third Hershey Conference on Developmental Cerebral Blood Flow and Metabolism. Dev Neurosci 24:364–366.

Hahn K, Prigarin S, Rodenacker K, Hasan K. 2009. Denoising for diffusion tensor imaging with low signal-to-noise ratios: method and Monte Carlo validation. Int J Biostat (In Press).

Hu X, Qiu J, Grafe MR, Rea HC, Rassin DK, Perez-Polo JR. 2003. Bcl-2 family members make different contributions to cell death in hypoxia and/or hyperoxia in rat cerebral cortex. Int J Dev Neurosci 21: 371–377.

Hu X, Nesic-Taylor O, Qiu J, Rea HC, Fabian R, Rassin DK, Perez-Polo JR. 2005. Activation of nuclear factor-kappaB signaling pathway by interleukin-1 after hypoxia/ischemia in neonatal rat hippocampus and cortex. J Neurochem 93:26–37.

Hu X, Rea HC, Wiktorowicz JE, Perez-Polo JR. 2006. Proteomic analysis of hypoxia/ischemia-induced alteration of cortical development and dopamine neurotransmission in neonatal rat. J Proteome Res 5:2396–2404.

Huang H, Zhang J, Wakana S, Zhang W, Ren T, Richards LJ, Yarowsky P, Donohue P, Graham E, van Zijl PC, Mori S. 2006. White and gray matter development in human fetal, newborn and pediatric brains. Neuroimage 33:27–38.

Huang H, Yamamoto A, Hossain MA, Younes L, Mori S. 2008. Quantitative cortical mapping of fractional anisotropy in developing rat brains. J Neurosci 28:1427–1433.

Huppi PS, Dubois J. 2006. Diffusion tensor imaging of brain development. Semin Fetal Neonatal Med 11:489–497.

Kamel M, Xie L-M, Xue L, Wosik J, Nesteruk K, Bockhorst K, Narayana PA. 2007. 7 Tesla very high SNR superconducting receive-only coil for rat brain imaging. Proc Int Soc Magn Res Med 2007: 327.

Kaminogo M. 1989. The effects of mild hyperoxia and/or hypertension on oxygen availability and oxidative metabolism in acute focal ischaemia. Neurol Res 11:145–149.

Kety SS, Schmidt CF. 1946. The effects of active and passive hyperventilation on cerebral blood flow, cerebral oxygen consumption, cardiac output, and blood pressure of normal young men. J Clin Invest 25: 107–119.

Koinig H, Williams JP, Quast MJ, Zornow MH. 2000. Effect of a neuronal sodium channel blocker on magnetic resonance derived indices of brain water content during global cerebral ischemia. Brain Res 887: 301–308.

Krageloh-Mann I, Toft P, Lunding J, Andresen J, Pryds O, Lou HC. 1999. Brain lesions in preterms: origin, consequences and compensation. Acta Paediatr 88:897–908.

Kuban KC, Leviton A. 1994. Cerebral palsy. N Engl J Med 330:188–195.

Kuker W, Mohrle S, Mader I, Schoning M, Nagele T. 2004. MRI for the management of neonatal cerebral infarctions: importance of timing. Childs Nerv Syst 20:742–748.

Larvaron P, Boespflug-Tanguy O, Renou JP, Bonny JM. 2007. In vivo analysis of the post-natal development of normal mouse brain by DTI. NMR Biomed 20:413–421.

Leahy FA, Cates D, MacCallum M, Rigatto H. 1980. Effect of CO_2 and 100% O_2 on cerebral blood flow in preterm infants. J Appl Physiol 48: 468–472.

Levison SW, Rothstein RP, Romanko MJ, Snyder MJ, Meyers RL, Vannucci SJ. 2001. Hypoxia/ischemia depletes the rat perinatal subventricular zone of oligodendrocyte progenitors and neural stem cells. Dev Neurosci 23:234–247.

Lundstrom KE, Pryds O, Greisen G. 1995. Oxygen at birth and prolonged cerebral vasoconstriction in preterm infants. Arch Dis Child Fetal Neonatal Ed 73:F81–F86.

Lyden PD, Krieger D, Yenari M, Dietrich WD. 2006. Therapeutic hypothermia for acute stroke. Int J Stroke 1:9–19.

Mader I, Schoning M, Klose U, Kuker W. 2002. Neonatal cerebral infarction diagnosed by diffusion-weighted MRI: pseudonormalization occurs early. Stroke 33:1142–1145.

Madi S, Hasan KM, Narayana PA. 2005. Diffusion tensor imaging of in vivo and excised rat spinal cord at 7 T with an icosahedral encoding scheme. Magn Reson Med 53:118–125.

Maneru C, Junque C, Salgado-Pineda P, Serra-Grabulosa JM, Bartres-Faz D, Ramirez-Ruiz B, Bargallo N, Tallada M, Botet F. 2003. Corpus callosum atrophy in adolescents with antecedents of moderate perinatal asphyxia. Brain Inj 17:1003–1009.

Meng S, Qiao M, Scobie K, Tomanek B, Tuor UI. 2006. Evolution of magnetic resonance imaging changes associated with cerebral hypoxia-ischemia and a relatively selective white matter injury in neonatal rats. Pediatr Res 59:554–559.

Mori S, Itoh R, Zhang J, Kaufmann WE, van Zijl PC, Solaiyappan M, Yarowsky P. 2001. Diffusion tensor imaging of the developing mouse brain. Magn Reson Med 46:18–23.

Mori S, Zhang J. 2006. Principles of diffusion tensor imaging and its applications to basic neuroscience research. Neuron 51:527–539.

Munkeby BH, Borke WB, Bjornland K, Sikkeland LI, Borge GI, Halvorsen B, Saugstad OD. 2004. Resuscitation with 100% O_2 increases cerebral injury in hypoxemic piglets. Pediatr Res 56:783–790.

Nagy Z, Lindstrom K, Westerberg H, Skare S, Andersson J, Hallberg B, Lilja A, Flodmark O, Lagercrantz H, Klingberg T, Fernell E. 2005. Diffusion tensor imaging on teenagers, born at term with moderate hypoxic-ischemic encephalopathy. Pediatr Res 58:936–940.

Nakajima S, Meyer JS, Amano T, Shaw T, Okabe T, Mortel KF. 1983. Cerebral vasomotor responsiveness during 100% oxygen inhalation in cerebral ischemia. Arch Neurol 40:271–276.

Nakata Y, Barkovich AJ, Wahl M, Strominger Z, Jeremy RJ, Wakahiro M, Mukherjee P, Sherr EH. 2009. Diffusion abnormalities and reduced volume of the ventral cingulum bundle in agenesis of the corpus callosum: a 3T imaging study. AJNR Am J Neuroradiol. 30:1142–1148.

Neil J, Miller J, Mukherjee P, Huppi PS. 2002. Diffusion tensor imaging of normal and injured developing human brain - a technical review. NMR Biomed 15:543–552.

Niermeyer S, Kattwinkel J, Van Reempts P, Nadkarni V, Phillips B, Zideman D, Azzopardi D, Berg R, Boyle D, Boyle R, Burchfield D, Carlo W, Chameides L, Denson S, Fallat M, Gerardi M, Gunn A, Hazinski MF, Keenan W, Knaebel S, Milner A, Perlman J, Saugstad OD, Schleien C, Solimano A, Speer M, Toce S, Wiswell T, Zaritsky A. 2000. International guidelines for neonatal resuscitation: an excerpt from the guidelines 2000 for cardiopulmonary resuscitation and emergency cardiovascular care: international consensus on xcience. Contributors and reviewers for the neonatal resuscitation guidelines. Pediatrics 106:E29.

Nishimura N, Iwasaki K, Ogawa Y, Shibata S. 2007. Oxygen administration, cerebral blood flow velocity, and dynamic cerebral autoregulation. Aviat Space Environ Med 78:1121–1127.

Olivier P, Baud O, Evrard P, Gressens P, Verney C. 2005. Prenatal ischemia and white matter damage in rats. J Neuropathol Exp Neurol 64:998–1006.

Paxinos G, Watson C. 2005. The Rat Brain in Stereotaxic Coordinates. Elsevier, Amsterdam.

Qiao M, Meng S, Scobie K, Foniok T, Tuor UI. 2004. Magnetic resonance imaging of differential gray versus white matter injury following a mild or moderate hypoxic-ischemic insult in neonatal rats. Neurosci Lett 368:332–336.

Regan RF, Kumar N, Gao F, Guo Y. 2002. Ferritin induction protects cortical astrocytes from heme-mediated oxidative injury. Neuroscience 113:985–994.

Rice D, Barone S Jr. 2000. Critical periods of vulnerability for the developing nervous system: evidence from humans and animal models. Environ Health Perspect 108:511–533.

Rice JE 3rd, Vannucci RC, Brierley JB. 1981. The influence of immaturity on hypoxic-ischemic brain damage in the rat. Ann Neurol 9: 131–141.

Rostrup E, Larsson HB, Toft PB, Garde K, Henriksen O. 1995. Signal changes in gradient echo images of human brain induced by hypo- and hyperoxia. NMR Biomed 8:41–47.

Rutherford MA, Cowan FM, Manzur AY, Dubowitz LM, Pennock JM, Hajnal JV, Young IR, Bydder GM. 1991. MR imaging of anisotropically restricted diffusion in the brain of neonates and infants. J Comput Assist Tomogr 15:188–198.

Saikumar P, Dong Z, Weinberg JM, Venkatachalam MA. 1998. Mechanisms of cell death in hypoxia/reoxygenation injury. Oncogene 17: 3341–3349.

Sakuma H, Nomura Y, Takeda K, Tagami T, Nakagawa T, Tamagawa Y, Ishii Y, Tsukamoto T. 1991. Adult and neonatal human brain: diffusional anisotropy and myelination with diffusion-weighted MR imaging. Radiology 180:229–233.

Schroeter M, Franke C, Stoll G, Hoehn M. 2001. Dynamic changes of magnetic resonance imaging abnormalities in relation to inflammation and glial responses after photothrombotic cerebral infarction in the rat brain. Acta Neuropathol 101:114–122.

Shimabuku R, Ota A, Pereyra S, Veliz B, Paz E, Nakachi G, More M, Oliveros M. 2005. Hyperoxia with 100% oxygen following hypoxia-ischemia increases brain damage in newborn rats. Biol Neonate 88:168–171.

Shin HK, Dunn AK, Jones PB, Boas DA, Lo EH, Moskowitz MA, Ayata C. 2007. Normobaric hyperoxia improves cerebral blood flow and oxygenation, and inhibits peri-infarct depolarizations in experimental focal ischaemia. Brain 130:1631–1642.

Sizonenko SV, Camm EJ, Garbow JR, Maier SE, Inder TE, Williams CE, Neil JJ, Huppi PS. 2007. Developmental changes and injury-induced disruption of the radial organization of the cortex in the immature rat brain revealed by in vivo diffusion tensor MRI. Cereb Cortex 17:2609–2617.

Song SK, Sun SW, Ramsbottom MJ, Chang C, Russell J, Cross AH. 2002. Dysmyelination revealed through MRI as increased radial (but unchanged axial) diffusion of water. Neuroimage 17:1429–1436.

Song SK, Sun SW, Ju WK, Lin SJ, Cross AH, Neufeld AH. 2003. Diffusion tensor imaging detects and differentiates axon and myelin degeneration in mouse optic nerve after retinal ischemia. Neuroimage 20: 1714–1722.

Stichel CC, Muller HW. 1998. The CNS lesion scar: new vistas on an old regeneration barrier. Cell Tissue Res 294:1–9.

Toet MC, Groenendaal F, Osredkar D, van Huffelen AC, de Vries LS. 2005. Postneonatal epilepsy following amplitude-integrated EEG-detected neonatal seizures. Pediatr Neurol 32:241–247.

Vannucci RC, Lyons DT, Vasta F. 1988. Regional cerebral blood flow during hypoxia-ischemia in immature rats. Stroke 19:245–250.

Vannucci RC, Connor JR, Mauger DT, Palmer C, Smith MB, Towfighi J, Vannucci SJ. 1999. Rat model of perinatal hypoxic-ischemic brain damage. J Neurosci Res 55:158–163.

Verma R, Mori S, Shen D, Yarowsky P, Zhang J, Davatzikos C. 2005. Spatiotemporal maturation patterns of murine brain quantified by diffusion tensor MRI and deformation-based morphometry. Proc Natl Acad Sci U S A 102:6978–6983.

Vexler ZS, Ferriero DM. 2001. Molecular and biochemical mechanisms of perinatal brain injury. Semin Neonatol 6:99–108.

Wahl M, Strominger Z, Jeremy RJ, Barkovich AJ, Wakahiro M, Sherr EH, Mukherjee P. 2009. Variability of homotopic and heterotopic callosal connectivity in partial agenesis of the corpus callosum: a 3T diffusion tensor imaging and Q-ball tractography study. AJNR Am J Neuroradiol 30:282–289.

Wang S, Wu EX, Tam CN, Lau HF, Cheung PT, Khong PL. 2008. Characterization of white matter injury in a hypoxic-ischemic neonatal rat model by diffusion tensor MRI. Stroke 39:2348–2353.

Watson NA, Beards SC, Altaf N, Kassner A, Jackson A. 2000. The effect of hyperoxia on cerebral blood flow: a study in healthy volunteers using magnetic resonance phase-contrast angiography. Eur J Anaesthesiol 17: 152–159.

Woods RP, Grafton ST, Holmes CJ, Cherry SR, Mazziotta JC. 1998a. Automated image registration: I. General methods and intrasubject, intramodality validation. J Comput Assist Tomogr 22:139–152.

Woods RP, Grafton ST, Watson JD, Sicotte NL, Mazziotta JC. 1998b. Automated image registration: II. Intersubject validation of linear and nonlinear models. J Comput Assist Tomogr 22:153–165.

Ye F, Xiang Q-S. Digital tuning to suppress ghost artifacts in EPI by minimization of total Variation. *In* Proceedings of the International Society for Magnetic Resonance in Medicine (ISMRM, ed.) p.1841. ISRM, Berlin, Germany.

Zaharchuk G, Martin AJ, Dillon WP. 2008. Noninvasive imaging of quantitative cerebral blood flow changes during 100% oxygen inhalation using arterial spin-labeling MR imaging. AJNR Am J Neuroradiol 29:663–667.

Zhang J, Richards LJ, Yarowsky P, Huang H, van Zijl PC, Mori S. 2003. Three-dimensional anatomical characterization of the developing mouse brain by diffusion tensor microimaging. Neuroimage 20:1639–1648.

Zhang J, Miller MI, Plachez C, Richards LJ, Yarowsky P, van Zijl P, Mori S. 2005. Mapping postnatal mouse brain development with diffusion tensor microimaging. Neuroimage 26:1042–1051.